Progress In Electromagnetics Research Letters, Vol. 92, 139–145, 2020

Wideband and Highly-Integrated Dual-Mode LTCC Filter Using Vertically Stacked Double-Ring Resonator

Liangfan Zhu*

Abstract—A wideband dual-mode band-pass filter (BPF) is proposed and implemented using a vertically stacked double-ring resonator (VSDR) and a pair of broadside-coupled input/output (I/O) feeding lines based on a 4-layer low temperature cofired ceramic (LTCC) substrate. The proposed BPF is required to cover the fifth generation (5G) N77/N78/N79 band (3.3–5 GHz), thus achieves a fractional bandwidth (FBW) of 40%. Furthermore, the proposed structure not only possesses a non-orthogonal I/O feeding style for convenient interconnection with neighboring devices, but also removes disturbing element for simpler layout. Comparison and discussion are implemented as well.

1. INTRODUCTION

Nowadays, the fifth generation (5G) mobile communication has been on its business operation with high-speed and high-capacity data transmissions. The 5G communication requires to use sub 6 GHz frequency spectrum to transmit wideband signals. The most promising bands for 5G new radio (NR) in frequency range 1 (FR1) are N77 (3.3–4.2 GHz), N78 (3.3–3.8 GHz), and N79 (4.4–5 GHz) [1, 2]. Therefore, there is an increasing requirement of 5G band-pass filters (BPFs), which are required to fulfill the needs of wideband characteristic, high integration, compact size, good performances, and convenient input/output (I/O) feeding. The proposed BPF in this letter is required to cover 5G N77/N78/N79 band, which is 3.3–5 GHz. Although modern dual-mode BPFs achieve a size reduction of 50% compared with single-mode ones, a large number of them suffer a limited bandwidth [3–6]. Furthermore, conventional dual-mode BPFs use orthogonal I/O feeding ports to excite two degenerate modes [7–9], which result in interconnecting difficulties with neighboring devices. Moreover, disturbing elements to excite two degenerate modes in conventional dual-mode BPFs take up a certain circuit space and increase the optimization work [10, 11].

In this paper, a dual-mode BPF is proposed to cover 5G N77/N78/N79 band. Owing to highly-integrated low temperature cofired ceramic (LTCC) technology, a vertically stacked double-ring resonator (VSDR) and a pair of broadside-coupled feeding I/O lines are vertically arrayed to achieve a wideband characteristic and a high level of integration. The merits of the proposed BPF include wideband characteristic, high level integration, non-orthogonal feeding, and no need of disturbing element.

2. CIRCUIT DESIGN AND ANALYSIS

2.1. Structure of the Proposed BPF

The structure of the proposed dual-mode BPF implemented on a 4-layer LTCC substrate is shown in Figure 1. Layers 1 and 3 are used to accommodate the I/O feeding lines, simultaneously, and

Received 15 May 2020, Accepted 16 July 2020, Scheduled 28 July 2020
* Corresponding author: Liangfan Zhu (zhuliangfan@hotmail.com).
The author is with the First Business Division, Anhui Huadong Photoelectric Technology Research Institute Co., Ltd, Wuhu High and New Technology Industry Development Zone, Anhui, China.

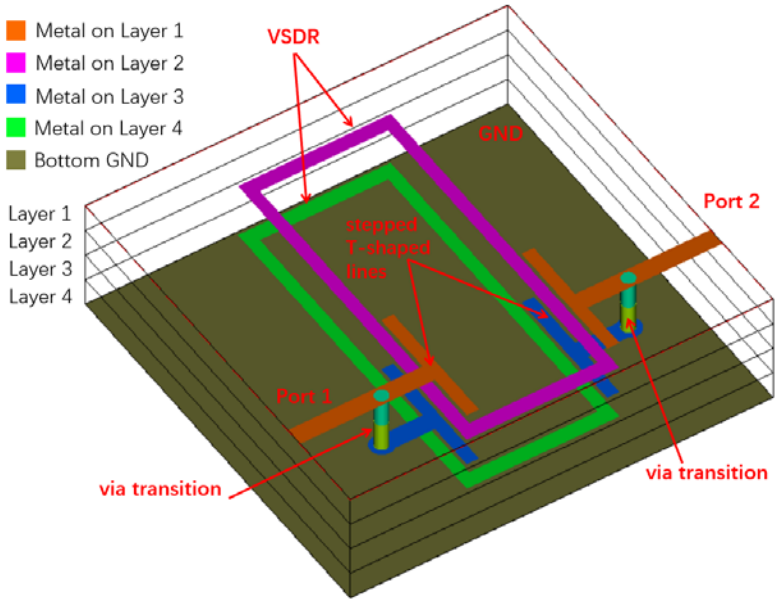

Figure 1. Structure of the proposed BPF.

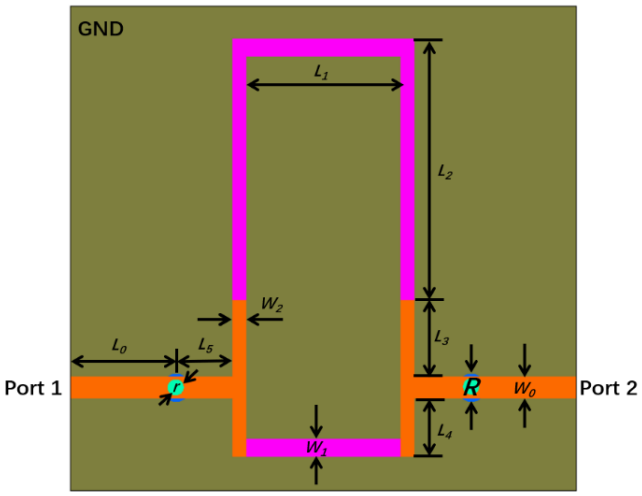

Figure 2. Plane geometry with parameters' definitions.

Layers 2 and 4 are used to accommodate VSDR. The 1st and 2nd rings of VSDR are placed on Layer 2 and Layer 4, respectively. For a strong coupling between the two rings of VSDR, the two rings are vertically stacked with broadside coupling effect. The I/O feeding lines use a stepped T-shaped structure on Layer 1, simultaneously, interconnected with another stepped T-shaped structure on Layer 3. The interconnections between the stepped T-shaped structures on Layer 1 and Layer 3 utilize via-interconnections. The VSDR and T-shape structures are interconnected with broadside-coupling effect as well, which helps enhance the bandwidth of the proposed BPF. The bottom metal is set to the ground layer. The plane geometry and dimensions' parameters of each section line are defined in Figure 2.

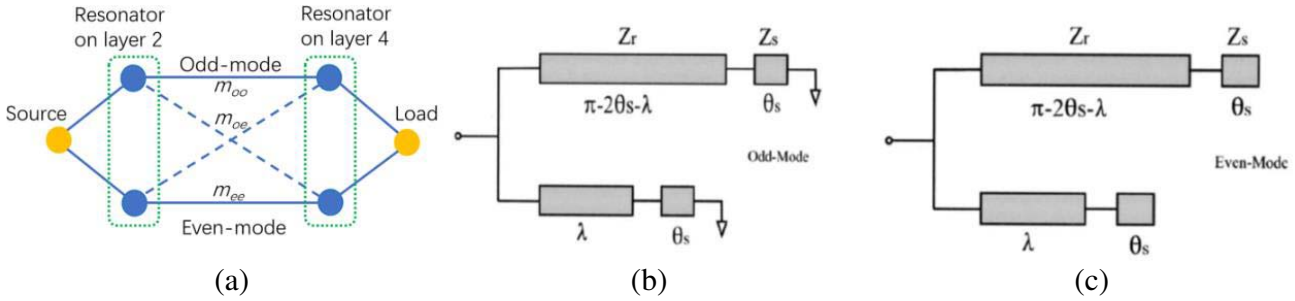

(a) (b) (c)

Figure 3. (a) Topology, (b) odd-mode and (c) even-mode circuit.

2.2. VSDR Design and Analysis

The topology of the proposed BPF is shown in Figure 3(a), where the yellow nodes represent source or load; blue nodes represent odd-mode and even-mode resonator; solid lines represent direct-coupling m_{oo} and m_{ee}, dashed lines represent cross-coupling m_{oe} between different modes of two resonators. The coupling strength of the two ring resonators is controlled by the width of resonator's line and the height between the two rings. The wider the line's width is, the stronger the coupling strength is. The less height (fewer layers) is between two rings, the stronger the coupling strength is as well. The VSDR can be analyzed by using its odd- and oven-mode equivalent circuits, respectively shown in Figures 3(b) and (c). The transmission characteristic equations are thus derived in Equations (1)–(4).

$$\tan(\theta_1 f_{no}) + 2D\tan(\theta_s f_{no}) - D^2\tan^2(\theta_s f_{no})\tan(\theta_1 f_{no}) = 0 \tag{1}$$

$$D^2\tan(\theta_1 f_{ne}) + 2D\tan(\theta_s f_{ne}) - \tan^2(\theta_s f_{ne})\tan(\theta_1 f_{ne}) = 0 \tag{2}$$

$$\theta_1 = \pi - 2\theta_s \tag{3}$$

$$D = \frac{Z_s}{Z_r} \tag{4}$$

where f_{no} and f_{ne} are the normalized odd- and even-mode frequencies; θ_s is the electrical length of the stepped T-shaped transmission line; and D is the impedance ratio. Equations (1)–(2) can be reduced to Equations (5)–(6) if one considers a case of a small step. Thus, it can be shown that the deviation from the normalized natural resonant frequency of the ring is approximately a linear function of the step angle for a given impedance ratio.

$$f_{no} = 1 + \frac{2\theta_s}{\pi}(1 - D) \tag{5}$$

$$f_{ne} = 1 - \frac{2\theta_s}{\pi D}(1 - D) \tag{6}$$

2.3. BPF Design and Analysis

The effective coupling between the stacked two rings is governed by the thickness h of VSDR, which in turn sandwiches the T-shaped coupled lines. Using the method in [12] of determining the loaded and unloaded Q-factor, Q_1, and Q_{u1}, respectively, the external Q-factor Q_e, Equations (7)–(8) are determined as a function of h in Figure 4:

$$Q_{u1} = \frac{Q_1}{1 - 10^{-\frac{L}{20}}} \tag{7}$$

$$Q_e = \frac{2Q_1Q_{u1}}{Q_{u1} - Q_1} \tag{8}$$

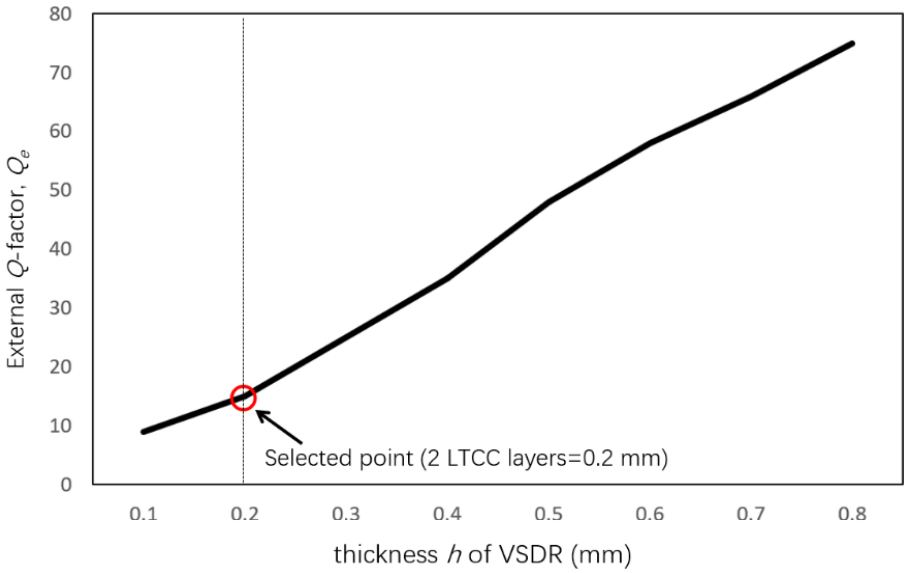

Figure 4. External Q-factor Q_e as a function of VSDR thickness h.

The proposed dual-mode BPF based on above topology is therefore specified and designed. The coupling k between the stacked two rings and external Q-factor Q_e of the BPF can thus be determined by using Equations (9)–(10).

$$k = \frac{\omega}{\sqrt{g_1 g_2}} \tag{9}$$

$$Q_e = \frac{g_0 g_1}{\omega} \tag{10}$$

Then center frequency and the bandwidth of the BPF are 4.15 GHz and 1.7 GHz, respectively. The normalized odd-mode and even-mode frequencies f_{no} and f_{ne} are selected to be 1.2 and 0.8, respectively. Using Equations (3)–(4), D and θ_s are calculated to be 0.3 and 0.4, respectively. The coupling coefficient k' between the split modes of the VSDR is then determined with Equation (11). The larger quantity of LTCC layers, the higher fabrication cost. With the considerations of balancing the integration level and fabrication cost, the line's widths (w_1 and w_2) and the layers' quantity between the two rings (h) of the VSDR are subsequently selected to be 0.32 mm and 0.2 mm, respectively.

$$k' = \frac{f_{no}^2 + f_{ne}^2}{f_{no}^2 - f_{ne}^2} \tag{11}$$

3. SIMULATED AND MEASURED RESULTS

The proposed BPF is fabricated on a 4-layer Ferro-A6 LTCC substrate. Each layer has a post-fired thickness of 0.1 mm with a dielectric constant of 5.9 and loss tangent of 0.002. AWR Microwave office simulator [13] and AXIEM solver [14] based on the full-wave electromagnetic (EM) simulation are used for the circuit simulation and electromagnetic (EM)-simulation, respectively. The dimension parameters are defined in Figure 2, and the optimal dimensions are listed in Table 1. A photograph of the proposed BPF is given in Figure 5(a). Ground-signal-ground (GSG) pads are reserved at the I/O ports for probe measurements. Measurements are carried out by Agilent N5230C network analyzer and Cascade Microtech Summit 9000 probe stations with 400 µm -GSG probes, shown in Figure 5(b). The circuit-simulated, EM-simulated and measured results are shown in Figure 6. The measured results are in a very good agreement with the simulated ones. It should be noted that the EM-simulated and the measured center frequencies are 4.15 and 4.11 GHz, respectively. The tiny frequency shift is caused by the ceramic shrinking after cofiring. The measured in-band S_{11} and S_{21} are better than -15 and -0.5 dB,

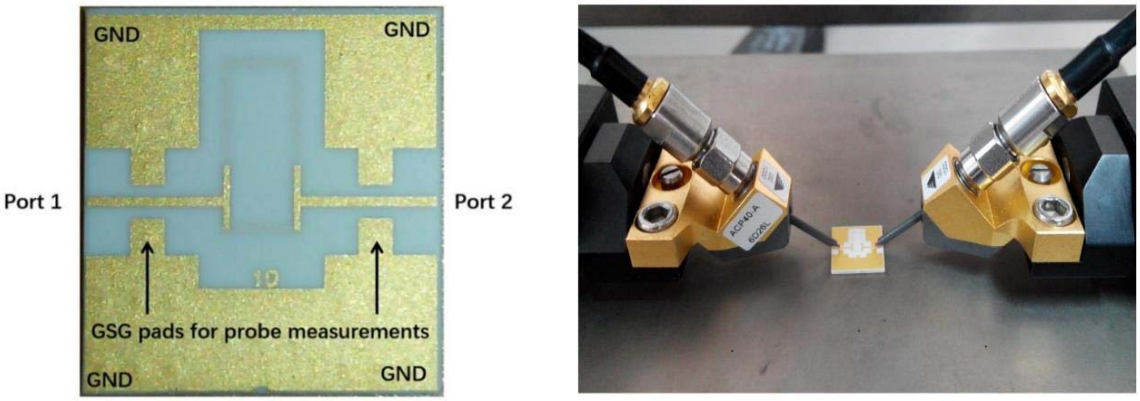

Figure 5. (a) Photograph of the proposed BPF and (b) photograph of the measurements with GSG-probes.

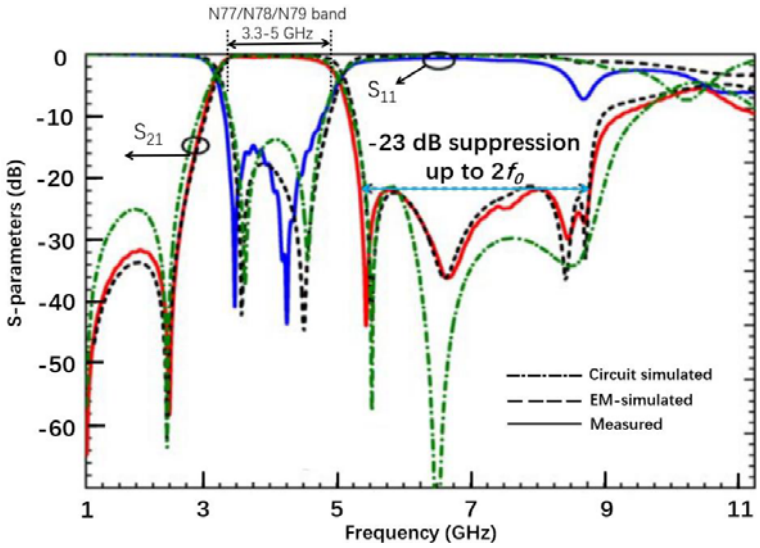

Figure 6. Simulated and measured S-parameters of the proposed BPF.

respectively. Notably, the proposed BPF has a wide upper band suppression of 23 dB up to the frequency of $2f_0$ (8.8 GHz). The size of the proposed BPF is only 5.2 mm × 5.66 mm or $0.14\lambda_g \times 0.24\lambda_g$, where λ_g is the guided wavelength at the center frequency of 4.15 GHz based on a 4-layer LTCC substrate. One transmission zero at 5.4 GHz is produced due to the crossing-coupling between two different modes of the cascaded resonators. The simulated transmission poles are located at 3.5 and 4.5 GHz, respectively. The measured transmission poles are at 3.4 and 4.25 GHz, respectively. The frequency shift of the transmission poles is caused by the LTCC material shrinking after co-firing.

Table 1. Dimensions of the proposed filters (unit: mm).

Parameter	L_0	L_1	L_2	L_3	L_4	L_5
Value	1.7	2.1	4.3	1.9	1.7	1.5
Parameter	W_0	W_1	W_2	r	R	
Value	0.55	0.32	0.32	0.3	0.6	

4. COMPARISON AND DISCUSSION

Comparison results between the proposed BPF and existing designs are summarized in Table 2. The overall performances of the proposed BPF exceed the performances of existing BPFs in terms of fractional bandwidth (FBW), in-band insertion loss, suppression at $2f_0$, I/O feeding style, size, integration level, and fabrication process [3–12]. Non-orthogonal I/O feeding style is very important for BPFs in transceiver's front-end systems, as the BPFs are required to be interconnected conveniently with neighboring devices. Conventional orthogonal I/O feeding may require larger circuit size and result in larger insertion loss as bend structures are need to be installed to change the directions I/O feeding lines. Disturbing element removing is also vital as the structure is simplified. The simplified BPF has less optimization work to do with fewer design parameters, and simplified BPF is suitable for mass productions.

Table 2. Performance comparison.

Refs.	Center frequency f_0 (GHz)	FBW	In-band insertion loss (dB)	Suppression at $2f_0$	I/O feeding style	Disturb element	Size ($\lambda_g \times \lambda_g$)	Level of integration	Fabrication process
3	9.1	11%	1.75	20 dB	Non-orthogonal	Needless	0.54×0.27	Medium	LTCC
4	73.8	5.5%	1.63	No	Non-orthogonal	Needless	0.39×0.31	High	LTCC
5	3.1	20.9%	1.65	20 dB	Non-orthogonal	Needless	0.75×0.4	Medium	PCB
6	5.35	15.9%	3.3	20 dB	Non-orthogonal	Needless	0.54×0.27	Low	LTCC
7	30	2.3%	1.91	No	Orthogonal	Need	0.62×0.55	Medium	LTCC
8	1.95	4%	2.8	No	Orthogonal	Needless	0.42×0.42	Low	PCB
9	5.22	5.1%	1.88	12 dB	Orthogonal	Need	0.29×0.29	Low	PCB
10	5.82	1.4%	1.6	12 dB	Orthogonal	Need	0.32×0.32	Low	PCB
11	2.45	20%	1.3	No	Non-orthogonal	Need	0.54×0.52	High	LTCC
This work	4.15	40%	0.5	23 dB	Non-orthogonal	Needless	0.14×0.24	High	LTCC

5. CONCLUSION

A dual-mode BPF for 5G applications is proposed and implemented based on a 4-layer LTCC substrate. The merits of the proposed BPF include wideband characteristic, high level integration, non-orthogonal feeding, and no need of disturb element. Comparison shows that the proposed BPF has better performances than existing dual-mode BPFs. The measured results are in a very good agreement with the simulated ones. The proposed BPF not only possesses good performances, but also has a simple structure. The simplified BPF is suitable for 5G mass production.

REFERENCES

1. Okuyama, Y. S. S. and N. I. T. Takada, "5G radio performance and radio resource management specifications," *NTT DOCOMO Technical Journal*, Vol. 20, No. 3, 2019.
2. Shin, K. R. and K. Eilert, "Compact low cost 5G NR N78 band pass filter with silicon IPD technology," *Proc. 2018 IEEE 19th Wireless and Microwave Technology Conference (WAMICON)*, 1–3, 2018.
3. Zhou, B., C. H. Cheng, L. Yan, N. Zhou, Y. Cao, Q. Tang, and Z. Wang, "Wide upper stopband and nonorthogonal I/O feed dual-mode LTCC filter," *Proc. 2016 IEEE IEEE International Symposium on Radio-Frequency Integration Technology (RFIT)*, 1–3, 2016.

4. Kuo, M. H., T. Y. Huang, H. Y. Tsai, C. X. Chen, and R. B. Wu, "A miniaturized bandpass filter using double folded dual-mode cavity resonators in LTCC," *Proc. 2015 Asia-Pacific Microwave Conference (APMC)*, Vol. 3, 1–3, 2015.
5. Rodríguez-Meneses, L. A., C. Gutiérrez-Martínez, R. S. Murphy-Arteaga, J. Meza-Pérez, and J. A. Torres-Fórtiz, "Wideband dual-mode microstrip resonators as IF filters in a K-band wireless transceiver," *Microwave and Optical Technology Letters*, Vol. 62, 606–614, 2020.
6. Chen, C.-H. and K.-H. Lin, "Novel compact chip design of 5 GHz LTCC dual mode 4 poles quasi-elliptic resonator filter," *Proc. 2007 Asia-Pacific Microwave Conference*, 1–4, 2007.
7. Ahn, K., M. Uhm, and I. Yom, "New circular-shaped dual-mode cavity for mm-wave filters using LTCC technology," *Proc. 2007 IEEE Antennas and Propagation Society International Symposium*, 2104–2107, 2007.
8. Zhao, F. L., M. H. Weng, C. Y. Tsai, R. Y. Yang, H. Z. Lai, and S. K. Liu, "A miniaturized high selectivity band-pass filter using a dual-mode patch resonator with two pairs of slots," *Microwave and Optical Technology Letters*, Vol. 62, No. 3, 1145–1151, 2020.
9. Ji, X.-B. and M. Yang, "Compact balanced bandpass filter with high selectivity based on two coupled dual-mode microstrip loop resonators," *Progress In Electromagnetics Research Letters*, Vol. 90, 143–149, 2020.
10. Rezaee, M. and A. R. Attari, "Analytical synthesis of coupling matrix for a dual mode dual band filter," *Microwave and Optical Technology Letters*, Vol. 59, No. 1, 80–83, 2017.
11. Zhan, Y., J. Chen, and H. Tang, "Miniaturized LTCC bandpass filter using transmission line dual-mode resonator," *Proc. 2014 IEEE International Workshop on Electromagnetics (iWEM)*, 22–23, 2014.
12. Chang, K., *Microwave Ring Circuits and Antennas*, John Wiley & Sons, Inc., New York, 1996.
13. Microwave Office, Applied Wave Research Corporation, El Segundo, CA.
14. AXIEM, Applied Wave Research Corporation, El Segundo, CA.